Natural Convection Heat Transfer of A Straight-fin Heat Sink

Xiangrui Meng[1,2], Jie Zhu[2,*], Xinli Wei[1,*], Yuying Yan[2]

[1] School of Chemical Engineering and Energy, Zhengzhou University, Henan, China

[2] Department of Architecture and Built Environment, The University of Nottingham, Nottingham, UK

ABSTRACT

The influence of mounting angle on heat dissipation performance of a heat sink under natural convection condition is investigated in this paper by numerical simulation and experimental test. It is found that the heat sink achieves the highest cooling power when its mounting angle is 90 °, while it reaches the lowest when the mounting angle is 15 °, which is 6.88% lower than that of 90 °. A heat transfer stagnation zone is the main factor that affects the cooling power of the heat sink, and its location and area vary with the mounting angle. It is identified that cutting the heat transfer stagnation zone is an effective way to improve the heat sink performance.

Keywords:

Natural Convection Heat Transfer, Heat Sink, Mounting Angle, Stagnation Zone

*Corresponding author. Email address: lazjz@nottingham.ac.uk (J. Zhu), xlwei@zzu.edu.cn (X. Wei).

1. Introduction

Heat sink is a passive heat exchanger that transfers heat generated by an electronic or a mechanical device to a fluid medium, such as air and liquid coolant. Heat dissipation is very important in the modern electronic industry, according to the statistical data, high temperature causes more than 55% failures of electronics [1]. The heat sink is also used in other areas, for example, heat dissipation of DSC (Dye-Sensitized Solar Cell) [2]. The heat sink has different structures, and can be classified into active and passive types. Compared to the active heat sink, the passive heat sink dissipates thermal energy through the nature convection, and usually it is made of aluminium finned radiator, so it has high reliability and low cost characters. The driving force in the passive heat sink is buoyancy force generated by temperature difference. The natural convection of heat sink can be divided into limited and infinite space convections according to the external space.

Most of the passive heat sinks have simple structure and low cost characters because of their straight fins. Elenbaas [3] carried out the earliest investigation on natural convective heat dissipation for a parallel fin heat sink, Bodoia and Osterle [4] deduced a theoretical solution of the natural convection heat dissipation for the parallel vertical fin heat sink on the basis of theoretical analysis. Other researchers studied and optimised the geometrical dimensions of parallel fin heat sink, and gave out some formulas for calculating geometrical dimensions [5-11]. Heat dissipation performance of the parallel straight fin heat sink can be improved by increasing air turbulence between the fins, such as arranging staggered cylinders [12], drilling holes on base plate [13], opening slots [14] or drilling holes on the fins [15].

The above studies are all conducted with the horizontal or vertical heat sink [16-18], nevertheless, the influence of the heat sink mounting angle on heat dissipation is rarely mentioned. Mehrtash et al. [19] studied the effect of inclination of fin-plate heat sink on heat dissipation by numerical simulation with three-dimensional steady-state natural convection. Based on Mehrtash's research results, Tari et al. [20] developed a Nusselt number formula, and found that the fin spacing is an important parameter affecting heat sink thermal performance [21]. Shen et al. [22] investigated heat dissipation properties of the heat sinks placed in eight different directions, and discovered that the denser the fin arrangement, the more sensitive the directionality. There are two main factors limiting the sink natural convection heat dissipation, one is that the heat transfer direction does not match with natural convection flow, and the other one is that the convection between the fins is blocked.

In this paper, the influence of heat sink mounting angle on its heat dissipation is investigated. A test rig is designed and built to measure heat dissipation performances of a heat sink at different mounting angles. The numerical simulation of the heat sink performance is carried out, and the simulation results are compared with the experimental data. The optimum mounting angle of the heat sink is obtained, which is useful for heat sink design and installation.

2. Experimental apparatus

2.1. General description

The main components of the test rig include a JP1505D DC power supply, a DC heating plate, an Agilent 34970A Data Acquisition, a number of K-type thermocouples and PT100 RTDs. The schematic of the test rig is shown in Fig. 1. The experimental system is located in a large closed space without the external interference to achieve the heat sink natural convection environment. A special support is designed to ensure the heat sink could rotate 360^{o} freely, as shown in Fig. 2. The heat sink and heating plate are fastened by bolts to reduce the contact thermal resistance and prevent the relative displacement between them. The heating plate is controlled by the JP1505D DC power supply for different heating powers. The maximum output power of the power supply is 750W, its output voltage range is from 0V to 150V with accuracy ± 0.3V and its current range is from 0A to 5A with accuracy ± 0.01A. The electric heating power is constant during the testing, the surface temperature of heat sink is measured and used to judge heat dissipation performance of the heat sink. The lower surface temperature of the heat sink, the better heat dissipation performance. Assuming heat is only dissipated by the heat sink when the temperature of the heat sink substrate became constant, the heat sink performance can be assessed by its surface temperatures.

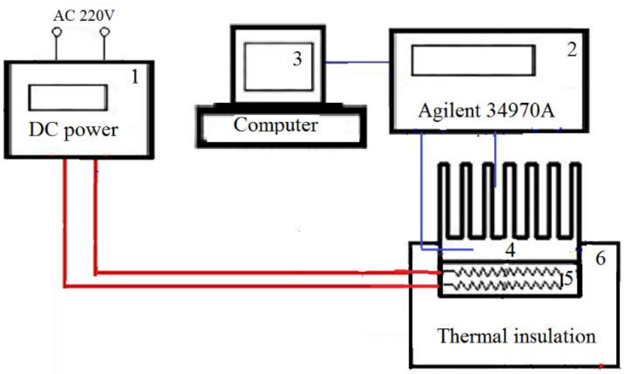

Fig. 1. Schematic of the test rig: (1) DC power; (2) Agilent 34970A; (3) computer; (4) heat sink; (5) heating plate; (6) thermal insulation

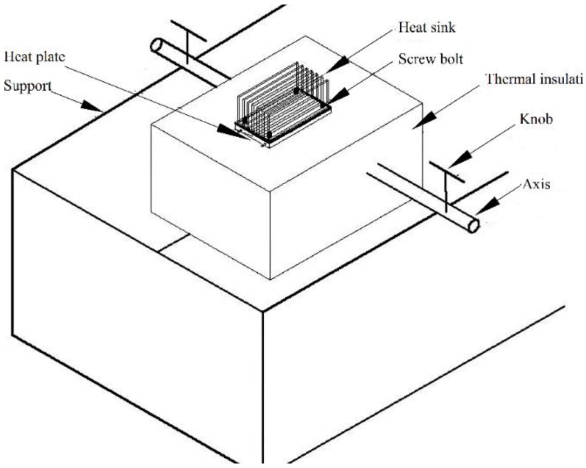

Fig. 2. Schematic of support

The data collection system consists of TC, RTD and Agilent 34970A Data Acquisition, the locations of the measuring points are shown in Fig. 3. TCs are set at Points 1 to 6 to get the heat sink bottom temperatures, RTDs are set at Points 7 to 9 to measure the fin surface temperatures. Agilent 34970A Data Acquisition with module 34902A, which features a built-in thermocouple reference and 16 two-wire channels, has 6 1/2-digit (22-bit) internal DMM and can scan up to 250 channels per second. The K-type armoured thermocouple WRNK-191 is used in the experiment. The material of WRNK-191 is nickel-chromium & nickel-silicon and its measurement temperature range is from 0^{o}C to 600^{o}C with accuracy ± 0.5^{o}C. Because of high thermoelectric power, the WRNK-191 TC has high sensitivity and its thermal response time is 3S. The measurement temperature range of SMD Pt100 RTD Temperature Sensor used for the fin surface is from -50°C to 200 °C with accuracy ± 0.15°C. It can be directly pasted to the fin surface with thermally conductive glue. The tested heat sink is an aluminium straight-fin type, its geometries are listed in Table1.

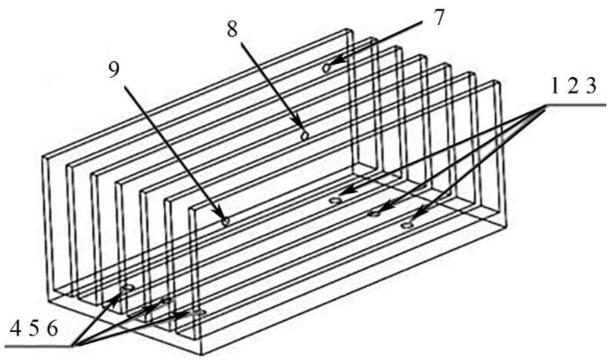

Fig. 3. Arrangement of measuring points. Points 1-6 K-type thermocouples; Points 7-9, PT100 RTDs

Table 1 The geometries of heat sink

Length (mm)	Width (mm)	Base thickness (mm)	Fin height (mm)	Fin thickness (mm)	Fins pitch (mm)	Number of fins
150	76	5	50	3	9.17	7

2.2. Experimental procedure

1) Coating thermal grease evenly on the heat sink bottom before fixing it to the heating substrate with screws.
2) Adjusting the mounting angle of the heat sink to a certain angle, and then checking the output voltage of DC power supply to insure the constant heating power.
3) The data of each measuring point are to be collected after the heat sink begin to be heated.
4) The equilibrium between heating and dissipation is reached as the maximum temperature fluctuate on the bottom surface of the heat sink substrate is less than 0.5^{o}C within 20 min.

The least thermal resistance method is used to assess the heat sink heat dissipation performance. Thermal resistance R_{th} can be calculated by following equation [5] :

$$R_{th} = \frac{T_{ave} - T_{sur}}{Q_{hs}} \tag{1}$$

Where T_{ave} and T_{sur} are the average temperatures of the heat plate and the ambient respectively, Q_{hs} is the heat dissipation power. With constant input power for the heat sink, the lower the thermal resistance, the higher the heat dissipation ability. Heat transfer coefficient h of the heat sink can be calculated from the following:

$$h = \frac{Q_{hs}}{A \cdot \Delta T} \tag{2}$$

Where A is heat sink surface area, ΔT refers to temperature difference between the heat sink surface and ambient.

2.3. Error Analysis

The experimental errors mainly include systematic and accidental errors. The error δ_y of a variable y can be obtained by the quadratic equation of the experimental data as the variables are assumed as $y=f(x_1, x_2, x_3, \cdots x_n)$:

$$\delta_y = \sqrt{(\frac{\partial y}{\partial x_1})^2 \delta x_1{}^2 + (\frac{\partial y}{\partial x_2})^2 \delta x_2{}^2 + \cdots + (\frac{\partial y}{\partial x_n})^2 \delta x_n{}^2} \tag{3}$$

Where, $x_1, x_2, x_3, \ldots x_n$ are independent variables, $\delta x_1, \delta x_2, \delta x_3, \ldots \delta x_n$ are their errors. The maximum errors of variables and measurement ranges are listed in Table 2. In addition, each test is repeated several times in order to minimise accidental errors, so the average data are likely to be close to the true values.

Table 2 Accuracies of sensors and the maximum relative errors of variables

	Temperature		Voltage	Current	Heating power	Thermal resistance
	TC	RTD				
Accuracy	± 0.5°C	± 0.15 °C	± 0.3V	± 0.01A	-	-

Maximum error	1.823%	1.367%	0.411%	0.909%	0.998%	2.08%

3. Numerical simulation model

The CFD simulation is carried out for the tested straight-fin heatsink using the symmetric model because the object is symmetric. The simulation zone is shown in Fig. 4 and its dimension is 900mm×456mm×330mm. Because of the regular geometric shape of the simulation zone, the hexahedral grid is adopted in the meshing procedure which will not only get high-quality grid but also be easy to modify the meshing strategy. The mesh density near the fin surface is increased for its $Y^+<1$ [23]. The simulation is carried out with different meshing strategies, the average surface temperatures of the fin are monitored and compared. The simulation results are shown in Fig. 5, it can be seen that the optimum meshing strategy is one with the grid number of 464058, and the optimum mesh model is shown in Fig. 6.

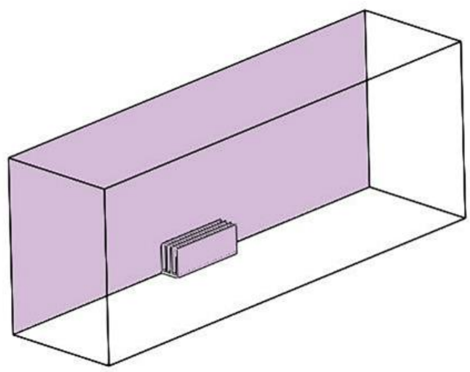

Fig. 4. Scope of the simulation

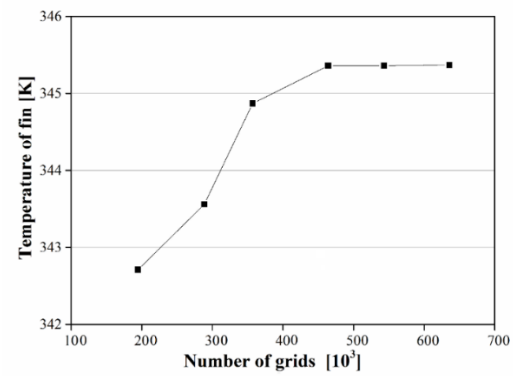

Fig. 5. Grid independence check

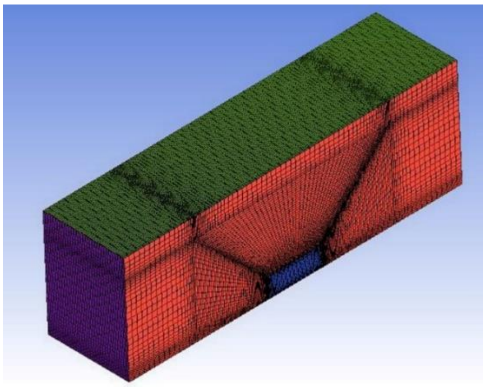

Fig. 6. Final meshed model

In order to reduce the amount of computational resources, the following assumptions are made:

1) The air flow is treated as a three-dimensional steady laminar flow.
2) Boussinesq model is used in air zone.
3) The temperature and heat flow of the heat plate are even.
4) Except density, the properties of air are constant.
5) Air is nonslip on the fin surface.
6) The viscous dissipation and radiation heat transfer are not considered.

3.1. Model for fluid region

Based on the mass conservation principle, the following continuity equation is adopted.

$$\frac{\partial(\rho u)}{\partial x}+\frac{\partial(\rho v)}{\partial y}+\frac{\partial(\rho w)}{\partial z}=0 \qquad (4)$$

Where ρ is air density, u, v, w are components of velocity, x, y, z are components of coordinate.

Energy equation is obtained on the basis of energy balance characteristics.

$$\frac{\partial(\rho uT)}{\partial x}+\frac{\partial(\rho vT)}{\partial y}+\frac{\partial(\rho wT)}{\partial z}=\frac{\kappa}{c_p}(\frac{\partial^2 T}{\partial x^2}+\frac{\partial^2 T}{\partial y^2}+\frac{\partial^2 T}{\partial z^2}) \tag{5}$$

Where T is air temperature, *k* is air thermal conductivity, *Cp* is air specific heat capacity.

The natural-convection flow is driven by the air density change and gravity force under heating condition. For external natural convection flow, the momentum equations can be written as:

$$\frac{\partial(\rho u^2)}{\partial x}+\frac{\partial(\rho uv)}{\partial y}+\frac{\partial(\rho uw)}{\partial z}=-\frac{\partial p}{\partial x}+\mu(\frac{\partial^2 u}{\partial x^2}+\frac{\partial^2 u}{\partial y^2}+\frac{\partial^2 u}{\partial z^2}) \tag{6}$$

$$\frac{\partial(\rho uv)}{\partial x}+\frac{\partial(\rho v^2)}{\partial y}+\frac{\partial(\rho vw)}{\partial z}=-\frac{\partial p}{\partial y}+\mu(\frac{\partial^2 v}{\partial x^2}+\frac{\partial^2 v}{\partial y^2}+\frac{\partial^2 v}{\partial z^2})+g(\rho-\rho_0) \tag{7}$$

$$\frac{\partial(\rho uw)}{\partial x}+\frac{\partial(\rho vw)}{\partial y}+\frac{\partial(\rho w^2)}{\partial z}=-\frac{\partial p}{\partial z}+\mu(\frac{\partial^2 w}{\partial x^2}+\frac{\partial^2 w}{\partial y^2}+\frac{\partial^2 w}{\partial z^2}) \tag{8}$$

Where *p* is air static pressure, μ is air viscosity.

3.2. Model for solid region

There is no internal heat source in the heat sink, so energy equation of solid region can be written as:

$$\frac{\partial^2 T}{\partial x^2}+\frac{\partial^2 T}{\partial y^2}+\frac{\partial^2 T}{\partial z^2}=0 \tag{9}$$

For natural-convection flow, the simulation can get quick convergence with the Boussinesq model,

$$\rho=\rho_0[1-\beta(T-T_0)] \tag{10}$$

Where ρ is air density at temperature T, ρ_0 is air density at T_0, β is air thermal expansion coefficient.

The interface between the fluid and solid domains is treated as the fluid-solid coupling surface, and no-slip condition is used for the fluid-solid boundary. The bottom of the heat sink is set as ‘WALL’ with a constant heat flux.

Low Reynolds number k-ε Turbulent Model is adopted in the simulation program because more accurate results can be obtained compared with the wall function method [24]. Especially, it can limit the error no more than 2% when coupled with full pressure outlet boundary condition. The other settings are Pressure based solver, SIMPLE algorithm, PRESTO! (Pressure Staggered Option) for pressure, Second order upwind format for other parameters. The residual value used as convergence indicator is 1e-06. The heat flux at the heat sink bottom and the fin surface temperature are also used as ancillary convergence indicators.

4. Results and discussion

4.1. Temperature distribution of heat sink

The fin temperature measurement results are listed in Table 3 at the mounting angle of 0^o. It can be found from this table, the fin bottom temperatures (Points 1-6 in Fig. 3) are almost same, but the surface temperatures (Points 7-9 in Fig. 3) are different. The surface temperature at the heat sink centre (Point 8) is obviously higher than those near the heatsink edge. As shown in Fig. 7, the temperature distributions of the heat sink fin and bottom are not uniform whether the mounting angle is 0^o or 45^o. At the mounting angle of 0^o, the highest temperature appears at the heat sink centre while the lowest temperature happens at the fin corner. The fin temperature in the middle of the heatsink is always higher than the others. This is consistent with the experiment results in Table 3. Compared with the mounting angle of 0^{o}, the highest temperature zone moves to the fin end edge at the mounting angle of 45^{o}.

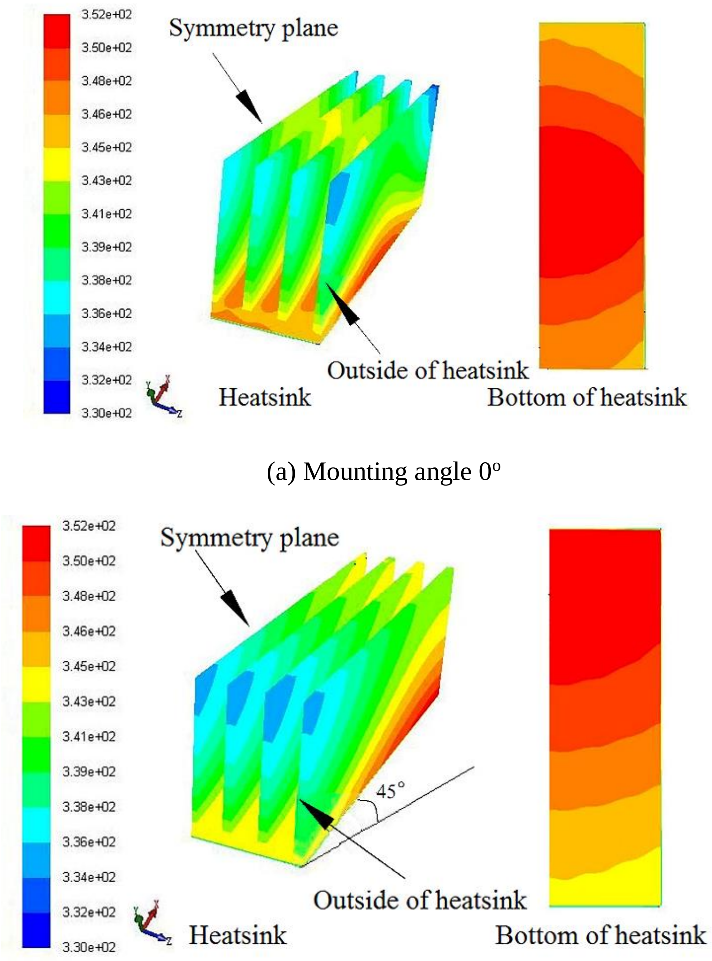

(a) Mounting angle 0^{o}

(b) Mounting angle 45^{o}

Fig. 7. Temperature contours of fin and bottom of heat sink with mounting angles 0^{o} and 45^{o}

Table 3 Fin temperatures at measuring points

Heating power (W)	Temperature at measuring point (^{o}C)									Average of bottom temperature (°C)
	1	2	3	4	5	6	7	8	9	
5	24	22	24	24	23	22	17	20	18	23.2
10	33	35	35	34	34	34	30	33	30	34.2

20	47	48	46	47	47	47	41	45	42	47
30	52	53	53	51	52	52	48	50	47	52.2
40	62	61	61	61	62	63	57	60	55	61.7
50	67	68	67	67	70	70	64	69	64	68.2
60	82	80	80	80	84	83	72	76	74	81.5
70	87	88	86	86	87	88	81	84	82	87
80	92	92	92	93	94	94	86	91	85	92.8

4.2. Influence of heating power on heat transfer coefficient

Heat transfer coefficients from simulation and experimental test are shown in Fig. 8 at the heat sink mounting angle of 0^{o}. It is found that the variation of simulation data is similar to that of experiment results. The maximum error between them is about 10.5% which is acceptable. Heat transfer coefficient increases rapidly with the heating power when the heating power is below 50W, but it increases moderately when the heating power is over 50W. The heat transfer driving force in the heat sink is the air flow, the air will get more heat from the heat sink as the heating power increases, and its flow velocity will increases as well, so the heat transfer coefficient becomes higher. The air flow resistance, however, will increase with the velocity, therefore the increase rate of heat transfer coefficient will decrease synchronously.

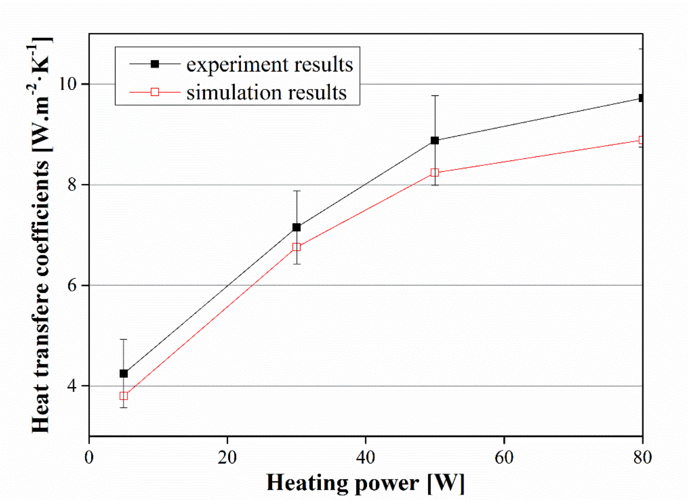

Fig. 8. Experimental and simulation results of heat transfer coefficient

4.3. Influences of heating power and mounting angle on thermal resistance

The variation of thermal resistance with the mounting angle is shown in Fig. 9. The thermal resistance increases with the mounting angle at first and reaches the maximum when the mounting angle is 15^{o}, then it decreases. The variation of thermal resistance is not significant when the mounting angle is over 60^{o}, it reaches the minimum when the mounting angle is 90^{o}. When heating power is higher than 50W, the fluctuation of thermal resistance is moderate, especially there is nearly no variation when the mounting angle is bigger than 60^{o}. The ratios between the maximum and minimum thermal resistances for the heating powers of 5W, 30W, 50W and 80W, are 29.78%, 18.12%, 6.88% and 13.98% respectively. So in practice, the mounting angle should be set as 90^{o}. The variation of thermal resistance with heating power is shown in Fig. 10. It is found that thermal resistance decreases with heating power. Thermal resistances at the mounting angle of 15^{o} are the biggest for all heating powers, while the resistances are the smallest and have no obviously different when the mounting angles are 60^{o}, 75^{o}, and 90^{o}.

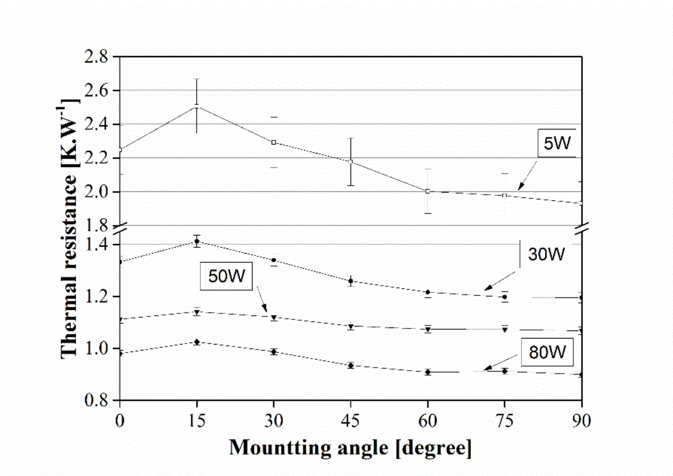

Fig. 9. Thermal resistance variation with mounting angle (experimental results)

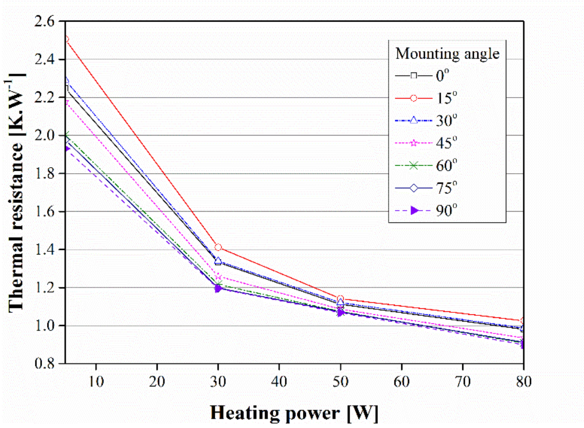

Fig. 10. Thermal resistance variation with heating power (experimental results)

4.4. Fluid temperature distribution and thermal resistance

Air streamlines and temperature distribution between the fins under 50W heating power condition are shown in Fig. 11. The variation of temperature contour has relevance to the fluid flow. The air flow direction moves to the upper side of the heat sink when the mounting angle increases. The position of the high-temperature zone changes following the fluid flow direction. The highest temperature always appears at the zone where the air flows out of the heat sink. The red zone in Fig. 11 represents that the air temperature is in the range from 70°C to 75°C. According to Fig. 7, the fin surface temperature at one zone is in the same range because of high thermal conductivity of the heat sink material, which means that the temperature difference between the fin and airflow is less than 5°C in this zone, calling it 'D zone' for easy identification. It also can be seen from Fig. 7 and Fig. 11 that in the other zones, the temperature difference between the fin and airflow is larger than 30°C, calling it 'A zone'. According to heat transfer equation $Q=hA\Delta T$, ΔT will be the key factor when h is kept constant or slightly fluctuate. Therefore, heat transfer in the 'D zone' will be very small compared to that in the 'A zone' and even can be ignored, so the 'D zone' is named as 'heat transfer stagnation zone'. The bigger the area of heat transfer stagnation zone, the lower the heat transfer. Then the area ratio (R_{hts}) of heat transfer stagnation zone to the fin is assessed. Fig. 12 shows R_{hts} variation with the mounting angle. It is found that the R_{hts} variation is similar to that of thermal resistance. They reach the maximum values at the mounting angle of 15°. The R_{hts} increases at first and then decrease sharply, afterwards it declines mildly. Fig. 12 confirms that the heat transfer stagnation zone is the main factor influencing the heat sink performance.

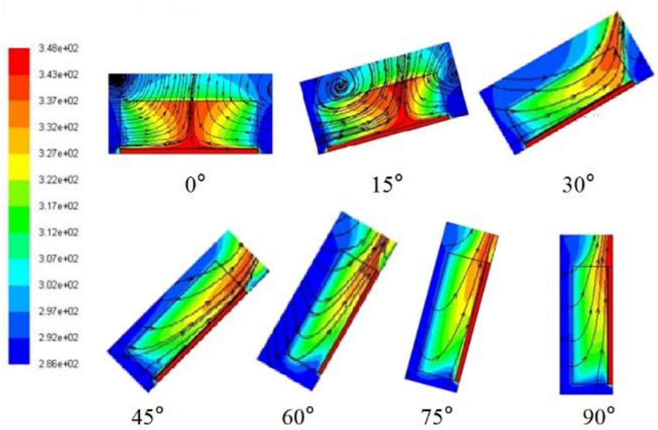

Fig. 11. Streamlines and temperature contours at different mounting angles

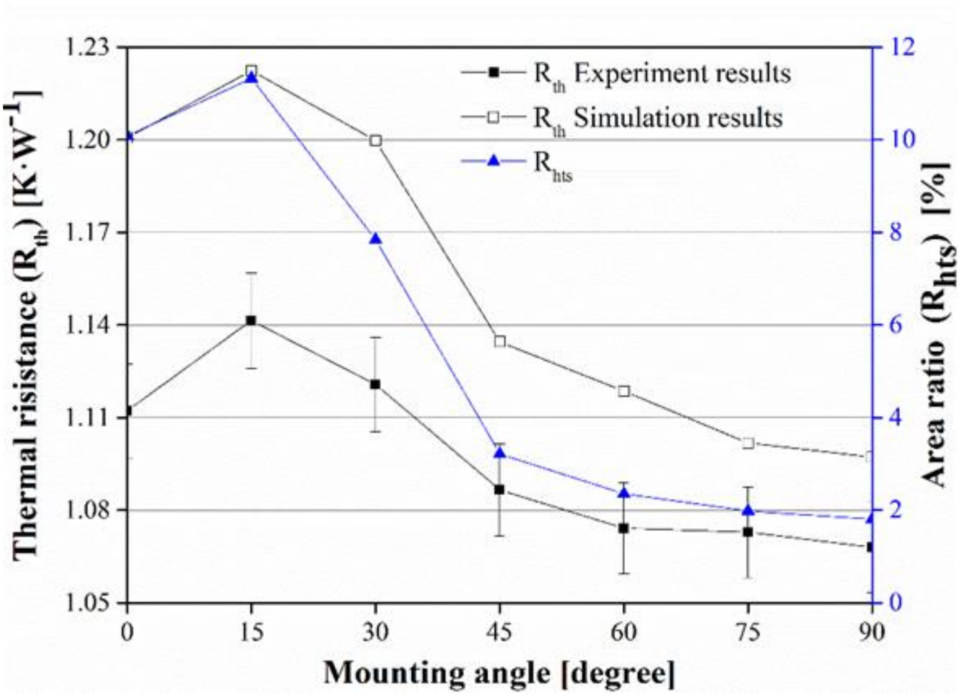

Fig. 12. Thermal resistance (R_{th}) and area ratio (R_{hts}) variations with mounting angle at 50W heating power

4.5. Cutting effect

The area and location of red zone change with the mounting angle as shown in Fig. 11. The location of red zone is just at the corner of the fin when the mounting angle is 30^o, so cutting this corner would decrease thermal resistance, this will confirm the inference that the heat transfer stagnation zone is the main aspect to affect the heat sink performance. Another reason for cutting this corner is that there is less influence on original air flow.

The new heat sink is shown in Fig. 13. The size of the cut corner is 20mm×20mm, the cut area takes up 2.5% of the whole fin area. The experimental results of the new heat sink at 50W and 80W heating powers are indicated in Fig. 14 and Fig. 15. It is found from Fig. 14 that the thermal resistance reduces about 2.64%~3.77% at heating power of 50W and 6.00%~10.13% at heating power of 80W. It is also found from Fig. 15 that the heat transfer coefficient increases about 7.30%~10.77% at heating power of 50W and 11.46%~17.07% at heating power of 80W. The variations of thermal resistance at the mounting angles of 0^o, 15^o and 30^o are smaller than those under other mounting angles. According to Fig. 11, this is in line with the previous assumption because the heat transfer stagnation zone is located at the fin corner.

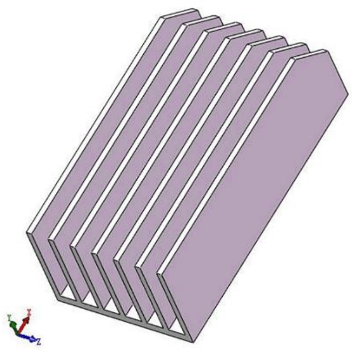

Fig. 13. 3D drawing of cut corner heat sink

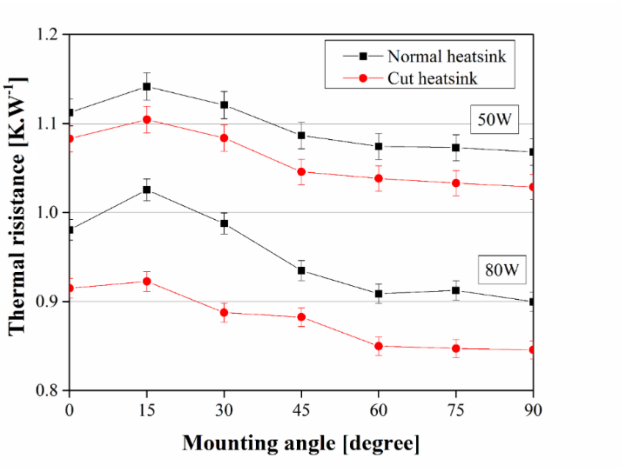

Fig. 14. Thermal resistance variation with mounting angle

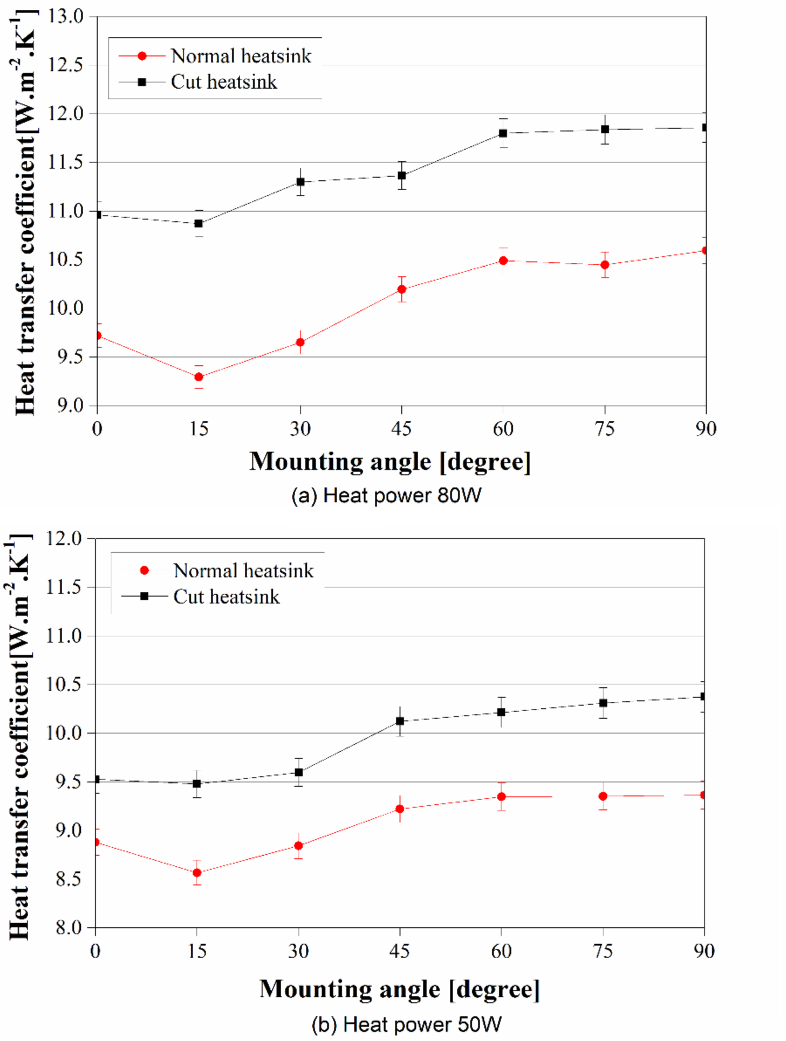

Fig. 15. Heat transfer coefficients at different mounting angles

5 Conclusion

Heat transfers of a straight fin heat sink under natural convection condition are investigated at different mounting angles in this paper. The heat sink surface temperatures are measured and used to judge its performance under constant heating power condition. The simulation results are verified by the experimental data with the maximum error less than 10.5%. The heat sink performance is the worst at the mounting angle of 15°, and the best performance happens at the angle of 90°. The heat transfer stagnation zone is identified where the temperature difference is less than 2°C in this study. The heat transfer stagnation zone area reaches the maximum when the mounting angle is 15°, that leads to the lowest performance because the effective heat dissipation area of the heatsink is the smallest. This is verified by cutting the corner portion of the heat sink where is the heat transfer stagnation zone. The heat transfer could be enhanced by cutting appropriate corner of the heat sink, the thermal resistance reduces 2.64%~3.77% at heating power of 50W and 6.00%~10.13% at heating power of 80W, and heat transfer coefficient increases 7.30%~10.77% at heating power of 50W and 11.46%~17.07% at heating power of 80W.

Conflict of interest

The authors declared that there is no conflict of interest.

Acknowledgements

Part of the work presented in this paper has received funding from the Scientific and Technological Planning Projects of Henan Province, China (No.162102310504). A part of this work was supported by the Foundation of State Key Laboratory of Coal Combustion (No.FSKLCC1410). The financial support is gratefully acknowledged.

Nomenclature

A heat sink surface area, m^2

c_p specific heat capacity of fluid, $J.kg^{-1}.K^{-1}$

h heat transfer coefficient, $W.m^{-2}\cdot K^{-1}$

k thermal conductivity, $W.m^{-1}.K^{-1}$

Q_{hs} heatsink input power, W

R_{th} thermal resistance, $K.W^{-1}$

R_{hts} the ratio of stagnation zone accounts for the fin whole area, dimensionless

T_{ave} average temperature of heat sink plate, K

T_{am} ambient temperature, K

ΔT temperature difference between heat sink surface and the ambient temperature, K

u, v, w components of velocity, $m.s^{-1}$

x, y, z components of coordinate

$x_1, x_2, x_3, \ldots x_n$ independent variables

$\delta x_1, \delta x_2, \delta x_3 \ldots \delta x_n$ errors of independent variables

Greek Symbols

β thermal expansion coefficient, K^{-1}

ρ air density, $kg.m^{-3}$

ρ_0 air density at T_0, $kg.m^{-3}$

μ viscosity, $N.s.m^{-2}$

References

[1]. S. Belhardj, S. Mimouni, A. Saidane, M. Benzohra, Using microchannels to cool microprocessors: a transmission-line-matrix study, Microelectron J. 34(4)(2003), 247-253.

[2]. H. Daniel, S. Bartolome, Y. Ryo, U. Satoshi, Y. Masafumi, K. Lars, S. Hiroshi, U. Satoshi, Liquid-Crystalline Dye-Sensitized Solar Cells: Design of Two-Dimensional Molecular Assemblies for Efficient Ion Transport and Thermal Stability, Chemistry of Materials 28(18)(2016) 6493-6500.

[3]. W. Elenbaas, Heat dissipation of parallel plates by free convection, Physica 9(1)(1942) 1-28.

[4]. J. R Bodoia, J. F. Osterle, The development of free convection between heated vertical plates, J. Heat Transf. 84(1) (1962) 40-43.

[5]. C. D Jones, L. F. Smith, Optimum Arrangement of Rectangular Fins on Horizontal Surfaces for Free-Convection Heat Transfer, Journal of Heat Transfer-Transactions ASME 92 (1) (1970) 6-10.

[6]. B. Yazicioğlu, H. Yüncü, Optimum fin spacing of rectangular fins on a vertical base in free convection heat transfer, Heat Mass Transfer. 44(1) (2007) 11-21.

[7]. H. K. Tae, H. D. Kyu, K. K. Dong, Closed form correlations for thermal optimization of plate-fin heat sinks under natural convection, Int. J. Heat Mass Transf. 54(5-6) (2011) 1210-1216.

[8]. J., Zhou, C., Yang, L. Zhang, Minimizing the entropy generation rate of the plate-finned heat sinks using computational fluid dynamics and combined optimization, Appl. Therm. Eng. 29 (8-9) (2009) 1872-1879.

[9]. S. Yu, K. Lee, S. Yook, Natural convection around a radial heat sink, Int. J. Heat Mass Transf. 53(13-14) (2010) 2935-2938.

[10]. S. Yu, K. Lee, S.Yook, Optimum design of a radial heat sink under natural convection, Int. J. Heat and Mass Transf. 54 (11-12) (2011) 2499-2505.

[11]. D. Jang, S. Yook, K. Lee, Optimum design of a radial heat sink with a fin-height profile for high-power LED lighting applications, Appl. Energy 116 (2014) 260-268.

[12]. M. A. Ismail, M. Z. Abdullah, M. A. Mujeebu, A CFD-based experimental analysis on the effect of free stream cooling on the performance of micro processor heat sinks, Int. Commun. Heat and Mass Transf. 35 (6) (2008) 771-778.

[13]. X. Yu, J. Feng, Q. Feng, Q. Wang, Development of a plate-pin fin heat sink and its performance comparisons with a plate fin heat sink, Appl. Therm. Eng. 25 (2-3) (2005) 173-182.

[14]. G. Huang, S. Wong, C. Lin, Enhancement of natural convection heat transfer from horizontal rectangular fin arrays with perforations in fin base, Int. J. Therm. Sci. (84) (2014) 164-174 .

[15]. M. Ahmadi, G. Mostafavi, M. Bahrami, Natural convection from rectangular interrupted fins, Int. J. Therm. Sci. (82) (2014) 62-71.

[16]. M. R. Shaeri, M. Yaghoubi, Thermal enhancement from heat sinks by using perforated fins, Energy Convers. Manage. 50 (5) (2009) 1264-1270.

[17]. D. S. Mangesh, M. Ashish, Natural convection heat transfer from a radial heat sink with horizontal rectangular fins, Int. J. Innovat. Res. Adv. Eng. 1(8) (2014) 353-356

[18]. R. G. Hamid, F. Mahdi, Mohammad M. N., Improvement of free convection heat transfer rate of rectangular heatsink on vertical Base plates. Energy and Power Eng., (3) (2011) 525-532.

[19]. M. Mehrtash, I. Tari, A correlation for natural convection heat transfer from inclined plate-finned heat sinks, Appl. Therm. Eng. 51(1-2) (2013) 1067-1075

[20]. I. Tari, M. Mehrtash, Natural convection heat transfer from horizontal and slightly inclined plate-fin heat sinks, Appl. Therm. Eng. 61(2) (2013) 728-736.

[21]. I. Tari, M. Mehrtash, Natural convection heat transfer from inclined plate-fin heat sinks, Int. J. Heat Mass Transf. 56 (1-2) (2013) 574-593.

[22]. Q. Shen, D. Sun, Y. Xu, T. Jin, X. Zhao, Orientation effects on natural convection heat dissipation of rectangular fin heat sinks mounted on LEDs, Int. J. Heat Mass Transf. 75 (2014) 462-469.

[23]. M. S. Salim, C. C. Siew, Wall y+ strategy for dealing with wall-bounded turbulent, IMECS 2009, Hong Kong, China, 2009, 2165-2170.

[24]. A. Mohd, M. S. Salim, C. C. Siew , Wall y+ approach for dealing with turbulent flow over a surface mounted cube: Part1-Low Reynolds Number, 7th International Conf. on CFD in the Minerals and Process Industries CSIRO, Melbourne, Australia, 2009,1-6.